Lecture 4

Fluid Mechanics Involving Interface

In this lecture, we will discuss the basic concepts of fluid mechanics involving the interface. To keep the discussion simple, we ignore all interfacial chemical reactions.

4.1 Interfacial coordinate system

For the interface between fluids A and B, there are two local vectors n (normal vector) and t (tangent vector) along the boundary line. n and t are equivalent to e_y and e_x of the local coordinate system, respectively. We define n pointing from A to B and t always on the right hand side orthogonal to n, as seen in Figure 4.1.

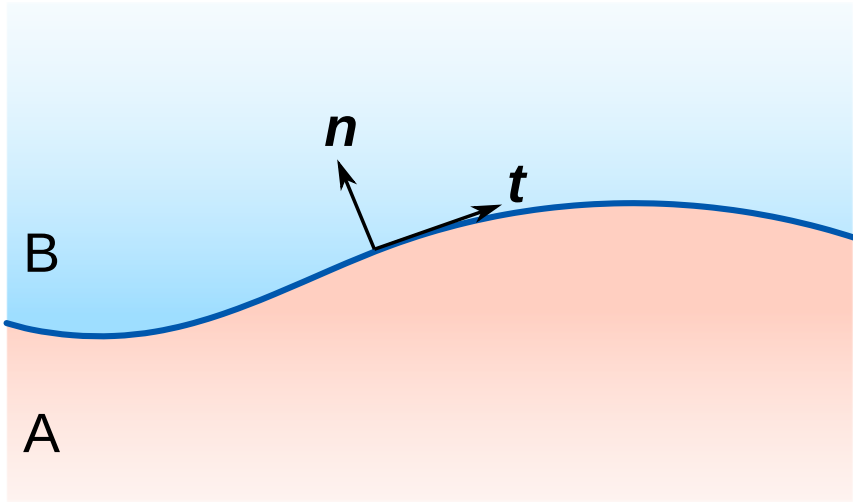

Figure 4.1: Normal vector n and t on the interface between A and B.

The velocities of both phases are v_A and v_B, respectively. The boundary conditions of v are:

- Tangential: no-slip boundary $v_A \cdot t = v_B \cdot t$

The no-slip boundary is a consequence of adhesion of molecules at the interface, and microscopically the outermost molecules at each phase do not move along the boundary line.[1,2] This is usually a convenient boundary condition for solid-liquid interface, however its limitation on real systems should also be noticed.[3,4]

- Normal: no-penetration boundary $v_A \cdot n = v_B \cdot n$

  This is easy to imagine since otherwise a non-zero normal velocity will make the boundary penetrate into one phase.

Using the local coordinate system on the interface, the stress balance at the boundary involving the pressure p, stress tensor τ is:[5]

- Normal component: $p_A - p_B + \tau_{nn}|_B - \tau_{nn}|_A + 2\mathcal{H}\gamma = 0$

  Here p is the pressure, τ_{nn} is the nn (yy)-component of the stress tensor τ, and $\mathcal{H} = -\frac{1}{2}(\nabla_s \cdot n)$ is the local mean curvature of the boundary. ∇_s is the surface gradient operator defined as $\nabla_s = \nabla - n(n \cdot \nabla)$.

- Tangential component: $\tau_{nt}|_B - \tau_{nt}|_A + t \cdot \nabla_s \gamma = 0$

  Here τ_{nt} is the nt (yx)-component of the Cauchy stress tensor.

At equilibrium, the normal components of the stress tensor balance each other, i.e. $\tau_{nn}|_A = \tau_{nn}|_B$. If there is no temperature change over the interface, $t \cdot \nabla_s \gamma = 0$ and we also have $\tau_{nt}|_A = \tau_{nt}|_B$. As a result the pressure difference across the interface is described by the surface tension and curvature:

$$p_A - p_B + 2\mathcal{H}\gamma = 0 \tag{4.1}$$

The surface curvature $\mathcal{H}$ can be expressed using the two principle radii R_1 and R_2 of the surface, as shown in Figure 4.2, with the equation:

$$|\mathcal{H}| = \frac{1}{2}\left(\frac{1}{R_1} + \frac{1}{R_2}\right) \tag{4.2}$$

For a spherical surface, $R_1 = R_2 = R$ and $|\mathcal{H}| = \frac{1}{R}$. The sign of $\mathcal{H}$ depends on the direction of n: when n points towards the local center of the curvature (where the center of the principle arc is), $H > 0$, and *vice versa* (Figure 4.3).

The relation of curvature can be used to explain several interesting phenomena. For example, the pressure inside a bubble is larger than the outside. Consider a gas bubble (A) in liquid (B). The normal vector n points from A to B and away from the center of curvature. Therefore $\mathcal{H} = -\frac{1}{R} < 0$. The pressure in liquid p_B is lower than p_A:

$$p_B = p_A - \frac{2\gamma}{R} \tag{4.3}$$

This is known as the Young-Laplace equation.[6] The pressure difference $\Delta p = p_A - p_B = \frac{2\gamma}{R}$ can be huge for micro- and nanoscale bubbles. For instance when R=1 μm, Δp is as

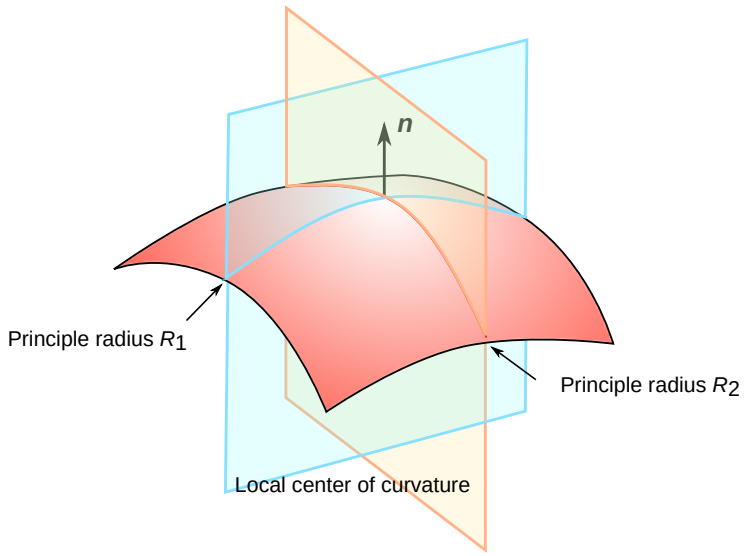

Figure 4.2: Scheme of the principle radii of a surface. For each point on the surface, the local curvature can be approximated by two arcs (shown in red and blue curves) with radii R_1 and R_2, called the principle radii.

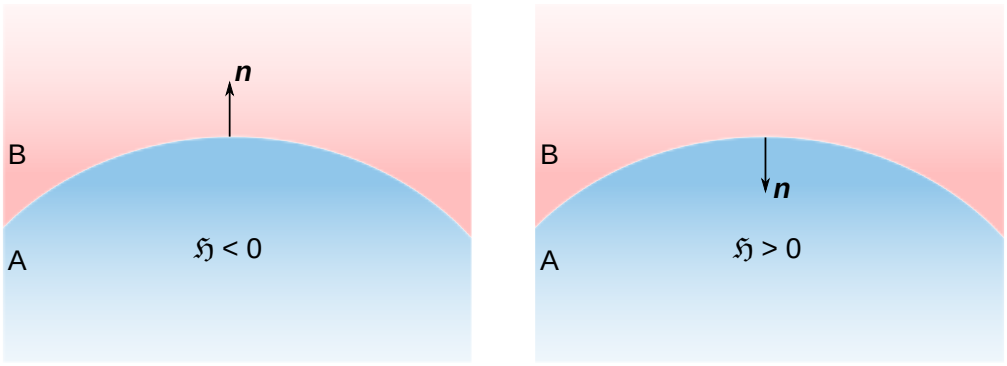

Figure 4.3: Sign of curvature $\mathcal{H}$ depends on the direction of n.

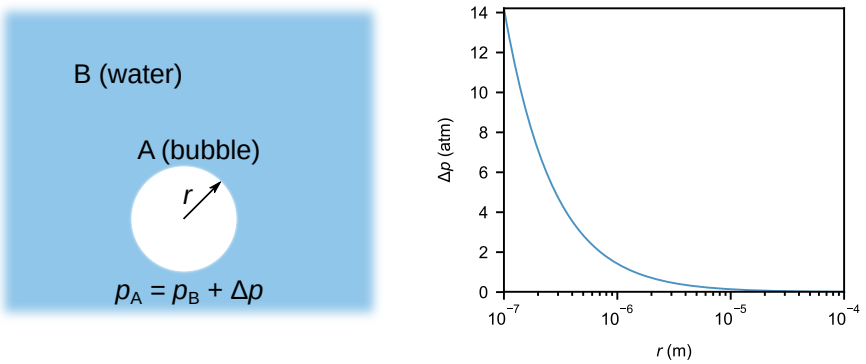

Figure 4.4: Pressure difference Δp between a gas droplet in water as a function of its radius R. Δp can be as huge as several atm when the bubble has a size below 1 μm.

high as 1.4 atm, while on the contrary when R=1 mm, Δp becomes only 144 Pa. The simulated pressure difference between a gas bubble and water as a function of its radius is shown in Figure 4.4. The simple analysis in Figure 4.4 indicates that nanobubbles (radius smaller than 1 μm) cannot survive due to the huge pressure imbalance. However recent evidence shows that such nanobubbles do exist and have even longer lifetime on a surface than we expected,[7] due to the effect of contact line pinning.

4.2 Meniscus near a Wilhelmy plate

Another example of interfacial fluid mechanics is the meniscus profile near a Wilhelmy plate. When the contact angle θ is smaller than 90° on the Wilhelmy plate, the cross section of the meniscus is a convex curve. If we set the liquid phase as A, and air as B, we know from our previous analysis that everywhere along the meniscus, $p_B(x) = p_A(x) + 2\mathcal{H}(x)\gamma$ and $\mathcal{H} > 0$. Very far from the interface $x \to \infty$, $p_B \approx p_A$, as shown in Figure 4.5. From another point of view, the pressure difference across the meniscus is caused by the hydrodynamic pressure. Since p_B is constant everywhere, $p_B = p_B(x \to \infty)$. Combine this with the hydrodynamic pressure in the liquid phase, $p_A(x) + \rho_L g h(x) = p_A(x \to \infty)$, we get:

$$p_B(x) = p_A(x) + \rho_L g h(x) \tag{4.4}$$

Follow the Young-Laplace equation, the relation between the local height and curvature is obtained as a differential equation:

$$\begin{aligned} 2\mathcal{H}(x) &= \frac{\rho_L g h(x)}{\gamma_L} \\ \frac{d^2h}{dx^2} &= \frac{\rho_L g h(x)}{\gamma_L}\left[\left(\frac{dh}{dx}\right)^2 + 1\right]^{\frac{3}{2}} \end{aligned} \tag{4.5}$$

which is derived from the equation of curvature in 1D.[5]

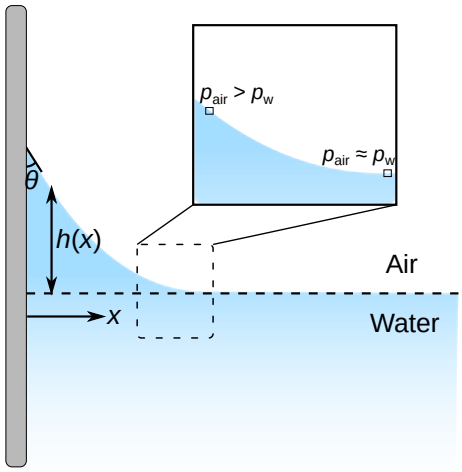

Figure 4.5: Meniscus near a Wilhelmy plate. Near the plate the pressure of air p_B is larger than the liquid pressure p_A due to local curvature, while far from the plate $p_A \approx p_B$.

We can use dimension analysis to get rid of ρ_L and γ_L. Since meniscus is an interplay between gravity and surface tension, we normalize h and x with the capillary length l (defined as $l = \sqrt{\frac{\gamma_L}{\rho_L g}}$). Using $H = h/l$ and $X = x/l$ as the normalized height and position, the dimensionless differential equation for the meniscus is then:

$$\frac{\mathrm{d}^2 H}{\mathrm{d}X^2} = B_o H \left[1 + (\frac{\mathrm{d}H}{\mathrm{d}X})^2\right]^{\frac{3}{2}} \tag{4.6}$$

where $B_o = \frac{\rho_L g l^2}{\gamma_L}$ is the Bond number (ratio between gravity and surface tension). The boundary conditions are:

$$\begin{cases} \frac{\mathrm{d}H}{\mathrm{d}X} = -\cot\theta & X = 0 \\ H = 0 & X \to \infty \\ \frac{\mathrm{d}H}{\mathrm{d}X} = 0 & X \to \infty \end{cases} \tag{4.7}$$

Therefore the meniscus profile can be solved numerically.

Some approximations can also be made to get an analytical solution. Since $\mathrm{d}H/\mathrm{d}X|_{X=0} = -\cot\theta$, when $\theta \sim 90°$, $\cot\theta \ll 1$. Equation 4.6 therefore reduces to a linear differential equation:

$$\frac{\mathrm{d}^2 H}{\mathrm{d}X^2} = B_o H \tag{4.8}$$

The solution of such equation is:

$$H(X) = \frac{\cot\theta}{\sqrt{B_o}} \exp(-\sqrt{B_o} X) \quad |\cot\theta| \ll 1 \tag{4.9}$$

which has the shape of exponential decay.

4.3 The coffee ring effect

Another interesting effect involving the interfacial fluid mechanics is the coffee ring effect. The coffee ring effect refers to the formation of ring-like pattern after the evaporation of a colloidal solution, which is typically observed in the stain from coffee. The coffee ring effect is associated with behavior of the contact line in an evaporating colloidal solution droplet. During the evaporation process of a pure liquid droplet, the contact angle θ remains at the receding angle θ_{rec}. However, θ of an evaporating colloidal solution droplet shows dependency with time t, as shown in Figure 4.6.

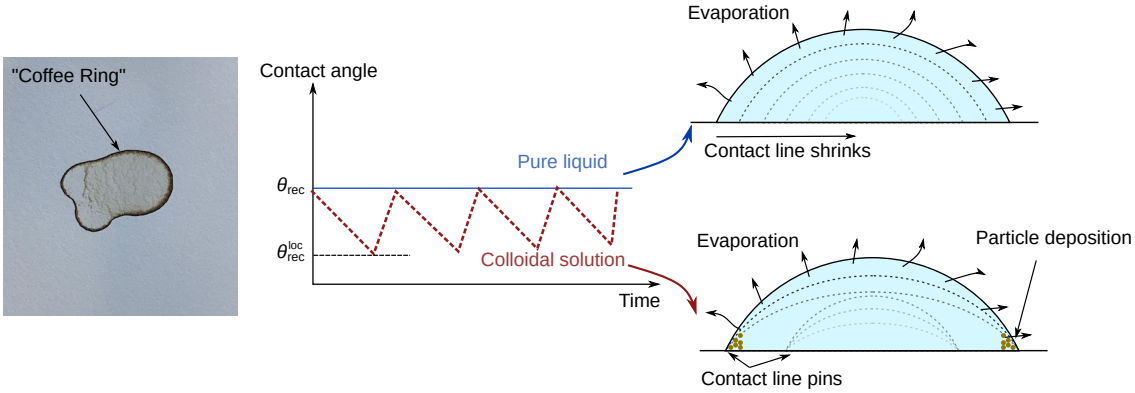

Figure 4.6: The coffee ring effect. The image shows a typical ring-like pattern when evaporating a colloidal solution. The contact angle of a droplet during evaporation is different between a pure liquid (contact angle remains constant) and a colloidal solution (contact angle changes with time). The lines in gray scale indicate the boundary of liquid during evaporation.

When the colloidal solution evaporates, particles get deposited along the contact line, which makes an energy barrier for the contact line to move inwards. This results in a phenomenon called "contact line pinning" and the contact angle reduces. When θ reduce below a certain angle $\theta_{\text{rec}}^{\text{loc}}$, the energy barrier is overcome, and the contact line shrinks again. Therefore θ reverts to θ_{rec} and another cycle of contact line pinning starts. After several cycles of pinning-releasing process, the deposited colloidal particles form a series of ring-like patterns.

The coffee ring effect can be seen as a transport problem involving 3 phase interfaces. The evaporation of a droplet can be seen as the time-dependent diffusion of (gaseous) solvent molecules, following Fick's second law:

$$\frac{\partial c}{\partial t} = \mathcal{D}\nabla^2 c \tag{4.10}$$

where $\mathcal{D}$ is diffusivity of water in air. The concentration profile can be solved assuming that the concentration near the droplet surface is the saturated vapor concentration, and far from the droplet $c = 0$. Here we will use the pseudo-steady state assumption (PSSA) to

get the concentration profile. From dimension analysis, the diffusion length scale is close to the radius of the droplet R and the characteristic time scale for vapor diffusion is:

$$t_{\mathrm{D}} \sim \frac{R^2}{\mathcal{D}} \tag{4.11}$$

We could also estimate the volume change of droplet, using the mass flux from Fick's first law:

$$\begin{aligned} \rho_{\mathrm{L}} \frac{\mathrm{d}V}{\mathrm{d}t} &= J \cdot A \\ m_{\mathrm{L}} \frac{R^3}{t_{\mathrm{V}}} &\sim \mathcal{D} \frac{\Delta c}{R} R^2 \end{aligned} \tag{4.12}$$

where $m_{\mathrm{L}} = \rho_{\mathrm{L}}/M$ is the concentration of molecules in the liquid. t_{V} is the characteristic time for the change of droplet volume. Compare Equations 4.11 and 4.12 we get the ratio between t_{D} and t_{V}:

$$\frac{t_{\mathrm{D}}}{t_{\mathrm{V}}} \sim \frac{\Delta c}{m_{\mathrm{L}}} \ll 1 \tag{4.13}$$

This means the time scale for the volume to change, t_{v} is much longer than the vapor molecules to diffuse, t_{D}. Therefore we can assume that $\nabla^2 c = 0$ in the vapor phase when studying the shape of the droplet. From the pseudo-steady profile of c in vapor, we can get the flux J at the droplet interface to solve the equation for droplet shape change. An example of the c and J profiles near a droplet using finite element analysis software is shown in Figure 4.7. The result of numerical simulations indicate that the diffusion flux is much larger near the three-phase contact edge, therefore a flow inside the droplet is induced. It turns out that a strong flux near the solid-liquid interface moves from the center to the edge. When colloidal particles are present in the solution, they are brought to the edge by such flow and deposited at the contact line. The deposited particles serve as a hydrophilic pattern which reduces the local receding angle $\theta_{\mathrm{rec}}^{\mathrm{loc}}$. Therefore the contact line is pinned until θ becomes lower than $\theta_{\mathrm{rec}}^{\mathrm{loc}}$ on the colloidal particles. When the contact line shrinks, the contact angle becomes θ_{rec} again. The process leaves a ring-like pattern of deposited colloidal particles on the solid surface, which is the coffee ring effect. In practical applications, the coffee ring is usually undesired when producing uniform colloidal film. The topic of engineering the coffee ring effect can be found in References [8–10].

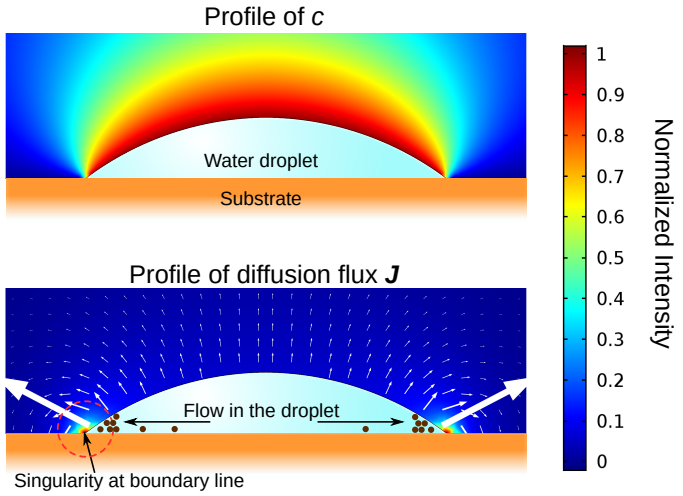

Figure 4.7: Example of the solution for c (upper) and J (lower) near an evaporating droplet using FEM software. The 2D color plots are normalized. For the diffusion flux, the intensity is shown using 2D color plot, while the arrows indicate both the intensity and direction of the flux. We can observe the singularity of diffusion flux near the contact line. As a result the flux inside the droplet brings the particles to the boundary line, which is the origin of the coffee-ring effect.

References

(1) Richardson, S. *J. Fluid Mech.* **1973**, *59*, 707.

(2) Shu, J.-J.; Teo, J. B. M.; Chan, W. K. *Soft Matter* **2016**, *12*, 8388–8397.

(3) Craig, V. S. J.; Neto, C.; Williams, D. R. M. *Phys. Rev. Lett.* **2001**, *87*, 054504.

(4) Zhu, Y.; Granick, S. *Phys. Rev. Lett.* **2002**, *88*, 106102.

(5) Deen, W. M., *Analysis of transport phenomena*, 2nd ed; Topics in chemical engineering; Oxford University Press: New York, 2012.

(6) Young, T. *Phil. Trans. R. Soc. of Lond.* **1805**, *95*, 65–87.

(7) Weijs, J. H.; Lohse, D. *Phys. Rev. Lett.* **2013**, *110*, 054501.

(8) Weon, B. M.; Je, J. H. *Phys. Rev. E* **2010**, *82*, 015305(R).

(9) Hu, H.; Larson, R. G. *J. Phys. Chem. B* **2006**, *110*, 7090–7094.

(10) Crivoi, A.; Duan, F. *Phys. Rev. E* **2013**, *87*, 042303.